Investigating gamma-ray bursts by joining Insight-HXMT and other gamma-ray spacecraft

C. Guidorzi*, R. Martone, M. Marongiu, F. Frontera, P. Rosati and E. Virgilli
Dept. Physics and Earth Science, University of Ferrara,
via Saragat 1, Ferrara, I-44122, Italy
**E-mail: guidorzi@fe.infn.it*

L. Amati, M. Orlandini and J. Stephen
INAF–OAS Bologna, Via Gobetti 93/3, Bologna, I-40129, Italy

C. Giuri
DESY, Platanenallee 6, Zeuthen, D-15738, Germany

S.-N. Zhang, S. Xiong
Institute of High Energy Physics, Chinese Academy of Sciences, Beijing, 100049, China

The Chinese mission Insight–HXMT allows for a high sensitivity study of the X-ray sky in 1250 keV, thanks to a smart combination of collimated detectors operating in different energy bands and providing a source location accuracy of 1 arcmin for a 20-σ source. In addition to observing Galactic sources, the HXMT High Energy (HE) instrument also operates in the so-called GRB mode, that makes it possible to detect and characterise GRB prompt emission from 200 keV to 3 MeV with an effective area as high as 2000 cm^2, thus filling the sensitivity gap of presently flying main GRB detectors in this energy range. We report the results of intensive simulations of the expected performances of HXMT for GRB science, showing how, especially in combination with, e.g., Swift/BAT and Fermi/GBM, the HXMT/HE will provide a significant improvement in the characterisation of temporal and spectral properties of the prompt emission of long GRBs, as well as an improved detection rate and better spectral characterisation of short GRBs.

Keyword: Gamma-ray bursts.

1. Introduction

The Insight Hard X-ray Modulation Telescope (HXMT) was launched June 15, 2017 in a 43°-inclination orbit and is devoted to X-ray astrophysics. The payload consists of three collimated instruments covering a total energy band of 1–250 keV[1]. The High–Energy instrument (HE), made of 18 phoswich detection units NaI(Tl) + CsI(NaI), operates in the 20–250 keV and has a total geometric area of $\sim$5000 cm^2, time resolution of 25μs and energy resolution of 19% at 60 keV. All the information for each photon is recorded. The detection system and the design of the HE units are very similar to those of the BeppoSAX/PDS instrument[2], thus making it an excellent instrument for the study of hard X-ray sources as well as a sensitive full-sky gamma-ray burst (GRB) monitor. In the normal operation mode, the energy band is 20–250 keV for NaI detectors and 40–600 keV for CsI detectors. The HE electronics and on-board data handling system are designed in such a way to identify NaI and CsI events, and to measure the energy of these events along with their occurrence time. In the normal mode, the CsI detectors above 100 keV exhibit an effective area ranging from few hundreds cm^2 for front incident radiation, to ∼1500–2000 cm^2, for radiation coming from the rear of the instrument. In the GRB operation mode, activated during Earth occultation of pointed sources, the HV of the HE instrument units is lowered to reduce the gain by a factor of ∼5, thus changing the energy band of the NaI detectors from 20–250 keV to 100–1250 keV and that of the CsI from 40–600 keV to 200–3000 keV (right panel of Fig. 1). In this paper we focus on the capabilities of HXMT/HE to detect and characterise the prompt emission of GRBs. In fact, the HE instrument is also operated in a GRB mode that allows to derive with high accuracy the temporal and spectral properties of the detected GRBs in the energy range from 200 keV to 3 MeV, thanks to an average effective area of ∼1500–2000 cm^2. This way, HXMT complements the sensitivities of other important and presently flying GRB detectors, like, e.g., Swift/BAT (15–150 keV) and Fermi/GBM (8 keV–30 MeV but with small effective area), thus providing a relevant contribution to the understanding of the physics of the prompt emission, one of the main open issues in the GRB field (e.g., see Ref. 3 for a review), and to the use of spectrum–intensity correlations for cosmology[4] (left panel of Fig. 1). For instance, the spectral peak energy, E_p, corresponding to the peak of the νF_ν spectrum, is a key parameter for GRB prompt emission models. In addition, E_p strongly correlates with the GRB radiated energy during the prompt emission[5,6], during the early X-ray afterglow[7], and with the time variability and properties of the power density spectrum of the gamma-ray time profile[8]. With

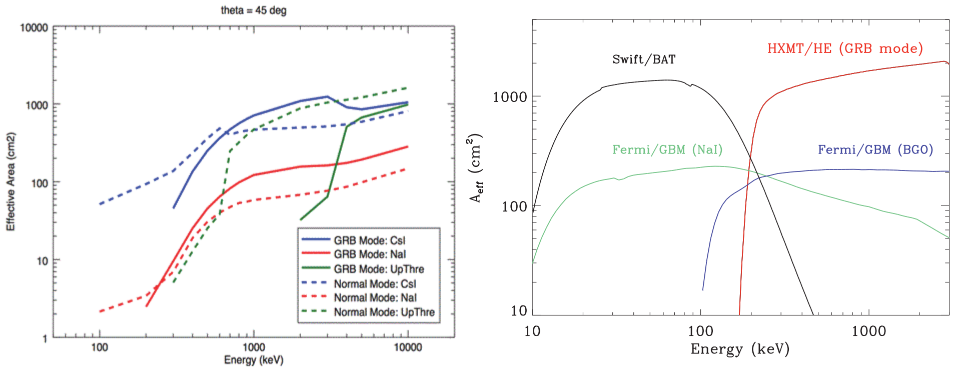

Fig. 1. *Left*: effective area of the NaI and CsI detectors of the HXMT/HE instrument in both normal and GRB modes, for an offset angle $\theta = 45°$ with respect to the detector axis. For each mode green lines show the efficiency of the high-energy threshold as a function of photon energy. The response function at different directions were determined through extensive Monte Carlo simulations (GEANT4) of the whole satellite. *Right*: effective area as a function of energy for Swift/BAT (on–axis), Fermi/GBM (sum of two NaI detectors and BGO, for a random direction in the sky) and HXMT/HE (GRB mode, $\theta = 135°$).

reference to the "Band function"[9], the high-energy spectral index β is also very important for testing and discriminating among various models, thus providing clues to the physics and geometry of the ultrarelativistic jet that is thought to act in a GRB. Swift/BAT measures mostly power-law spectra, thus providing estimates of E_p only for a few GRBs and almost no estimates of β, whilst most Fermi/GBM spectra can be fitted with a cut-off power-law, with no clues on β.

2. GRB spectroscopy

We quantified the improvements expected by joining HXMT/HE with other missions through simulations with the XSPEC package (v.12) in terms of the accuracy in determining E_p and β. The response matrix of HXMT/HE in GRB mode was obtained through intensive Monte Carlo simulations of the instrument and of the whole satellite, combined with extensive on-ground calibrations[1]. We used the response matrix for an offset incident angle of $\theta = 135°$, which is the rear side direction. The background spectrum was derived by taking into account the expected in-flight background components, including CXB, primary and albedo protons, electrons and positrons, gamma-rays albedo and SAA proton activated fluorescence by instrument and satellite structures[10]. Figure 2 (*left*) shows the Swift/BAT (measured) and HXMT/HE (simulated) joint spectrum of the medium intensity GRB 161218A. While BAT alone would measure a simple power-law spectrum, the HE data are essential to constrain both E_p and β by measuring the whole spectral curvature. A comparison between Fermi/GBM and HXMT/HE spectral capabilities is also shown (*right*): we simulated the spectrum of a medium–weak GRB (10–1000 keV fluence of 5×10^{-6} erg cm^{-2}) with a typical Band spectral shape: $\alpha = -1$, $\beta = -2.3$ and $E_\mathrm{p} = 300$ keV. In particular, we simulated the spectra of the two NaI detectors and

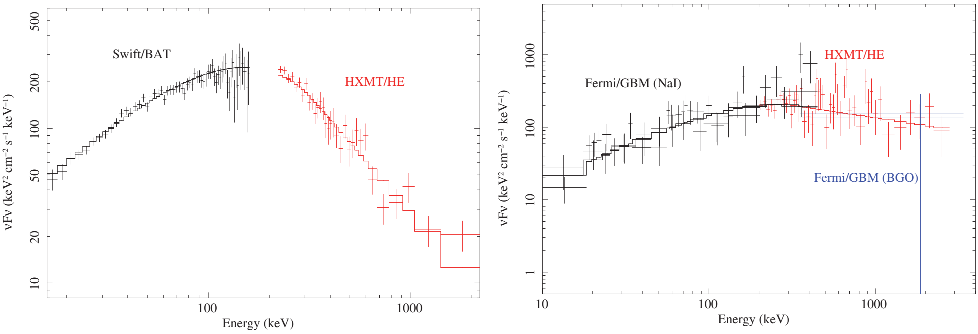

Fig. 2. Left: νF_ν spectrum of GRB 161218A as measured by Swift/BAT and expected with HXMT/HE (GRB mode) by assuming the spectral parameters measured by Konus–WIND[11]. Right: simulated Fermi/GBM and HXMT/HE (GRB mode) spectra of a medium–weak GRB (10–1000 keV fluence of 5×10^{-6} erg cm^{-2}) with a typical Band spectral shape with $\alpha = -1$, $\beta = -2.3$ and $E_\mathrm{p} = 300$ keV and 25-s duration. Channels have been grouped to ensure $> 2\sigma$ significance.

the BGO detector most illuminated by the considered GRB, as usual with real data. Although the nominal energy band of the GBM extends up to 20–30 MeV, its effective area is poor with respect to that of HXMT/HE at energies higher than ∼300 keV (Fig. 1). Thus, also in this case HXMT/HE data are essential to constrain the spectral shape and determine $E_{\rm p}$ and β. We then simulated a set of Fermi/GBM (using real background data) and HXMT/HE (GRB mode) spectra by assuming the above typical spectral shape and a 10–1000 keV fluence in the range 10^{-4}–10^{-7} erg cm^{-2}. The results are shown in Fig. 3 in terms of fractional 1σ uncertainty in the estimates of $E_{\rm p}$ and β as a function of GRB fluence. Clearly, HXMT/HE alone constrains $E_{\rm p}$ well only for the brightest GRBs, whereas β is measured well down to the faintest ones. Conversely, the Fermi/GBM alone constrains $E_{\rm p}$ down to medium-bright GRBs. Yet, only the joint analysis of both instruments enables a good estimate of $E_{\rm p}$ down to fluences as low as 5×10^{-7} erg cm^{-2}. This will significantly increase the number of GRBs that can be used for testing prompt emission models and for the study of the $E_{\rm p}$–intensity correlations. For progressively lower GRB fluences and higher values of $E_{\rm p}$ the HXMT spectral capabilities become increasingly relevant, especially for short GRBs, whose average $E_{\rm p}$ is higher than that of long ones[12].

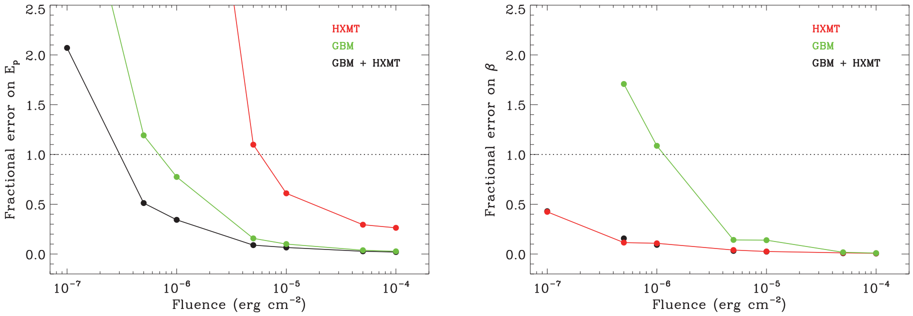

Fig. 3. Fractional error on spectral parameters $E_{\rm p}$ (*left*) and β (*right*) as a function of fluence (10–1000 keV) for a GRB with $\alpha = -1$, $\beta = -2.3$ and $E_{\rm p} = 300$ keV, and duration 25 s, as would be measured with Fermi/GBM alone, HXMT/HE alone and a joint spectral analysis of spectra from the two instruments.

3. GRB timing

The degree of variability exhibited by GRB light curves is long known to be related to luminosity[13,14] and spectral properties[8]. Among the various characterising temporal observables, such as the average[15] and the individual power density spectrum[8,16], noteworthy is the so-called spectral (or "time") lag, i.e. the delay between the time profiles of a given GRB at two different energy channels with softer photons lagging behind harder ones. The spectral lag is important for several aspects: (i) it anti-correlates with luminosity for long GRBs[17,18] as well as for GRB X-ray flares[19]; (ii) it discriminates between long and short GRBs, for which typical values are several ten or hundred ms vs. just a few ms, respectively[20]; (iii) an exhaustive self-consistent explanation is still missing, although two main interpretations have been put forward: (a) a spectral hard-to-soft evolution within the fluid comoving frame, or (b) a kinematic/geometric effect due to the Doppler factor connected with the bulk Lorentz factor of the jet, or the combination of both. The spectral lag is usually calculated through the cross-correlation function (CCF) of the two profiles. As such, its accuracy strongly depends on the number of counts, especially in the harder channel, which is more significantly hampered by low-count statistics: indeed, above > 300 keV the lag calculation is an almost uncharted territory, apart from rare, exceptionally bright events. This limitation is even more severe for short GRBs due to the lower fluence and harder photons than for long GRBs. Thanks to its large effective area above a few hundreds keV, HXMT/HE holds a great promise for the spectral lag calculation even for less fluent GRBs, such as short ones. We assessed the potential of joining HXMT/HE to Fermi/GBM through a number of simulations of short GRB profiles, assuming the response function for an off axis angle of $\theta = 135°$ in GRB mode. In particular, we simulated a fast-rise exponential decay (FRED) with an instantaneous spectrum described by a Band function with typical values for short GRBs: $\alpha = -0.5$, $\beta = -2.3$, and $E_{\rm p}$ monotonically decreasing from the initial value of 1 MeV according to Ref. 21. Figure 4 shows

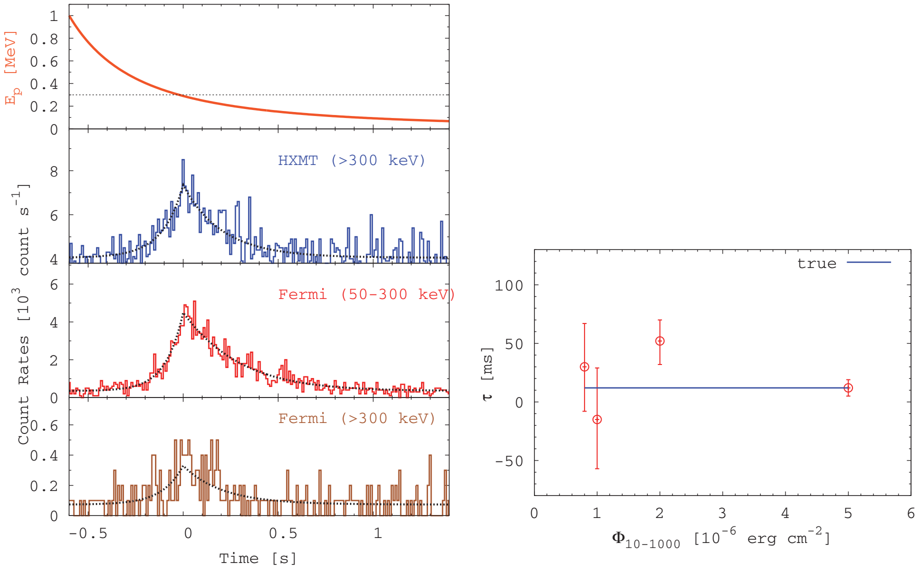

Fig. 4. *Left*: simulated profile of a short GRB ($T_{90} = 0.84$ s; 10–1000-keV fluence of 5×10^{-6} erg cm^{-2}) with hard-to-soft evolution due to a decreasing $E_{\rm p}$ (top). The HXMT/HE profile above 300 keV is shown in comparison with the Fermi/GBM soft (50–300 keV) and hard (> 300 keV) bands. In the hard channel the better statistical quality of HXMT/HE is evident. *Right*: spectral lag between HXMT/HE (> 300 keV) and Fermi/GBM (50–300 keV) profiles as a function of the 10–1000-keV fluence of the short GRB, compared with the true value (solid line).

the different simulated profiles for HXMT/HE and for Fermi/GBM (*left*), where the statistical quality of the latter is clearly lower than that of the former. We then calculated the lag via CCF between the soft energy channel of Fermi/GBM and that of HXMT/HE for a number of identically shaped short GRBs within increasing γ–ray fluences and compared the results with the true value (measured without statistical noise): the result (right panel) shows the unprecedented good accuracy obtained at any given fluence in the considered range. This will allow for a better characterisation of the spectral lag of a larger number of short GRBs, whose relevance cannot be overstated given their association with the mergers of binary neutron stars revealed through the detection of gravitational waves, as was first the case for GRB170817A/GW170817[22].

Acknowledgments

We acknowledge financial contribution from the agreement ASI-INAF n.2017-14-H.0.

References

1. S. Zhang, F. J. Lu, S.N. Zhang, T.P. Li, *Procs. SPIE*, **9144**, 914421 (2014).
2. F. Frontera, E. Costa, D. Dal Fiume, et al., *A&AS*, **122**, 357 (1997).
3. P. Kumar and B. Zhang, *Physics Reports*, **561**, 1 (2015).
4. L. Amati and M. Della Valle, *Int. J. of Mod. Phys. D*, **22**, 30028 (2013).
5. L. Amati, F. Frontera, M. Tavani, et al., *A&A*, **390**, 81 (2002).
6. R.-J. Lu, J.-J. Wei, E.-W. Liang et al., *ApJ*, **756**, 112 (2012).
7. M. G. Bernardini, R. Margutti, E. Zaninoni, et al., *MNRAS*, **425**, 1199 (2012).
8. S. Dichiara, C. Guidorzi, L. Amati, et al., *A&A*, **589**, A97 (2016).
9. D. Band, J. Matteson, J. Ford et al., *ApJ*, **413**, 281 (1993).
10. F. Xie, J. Zhang, L.-M. Song et al., *Ap&SS*, **360**, 47 (2015).
11. D. Fredericks, S. Golenetskii, R. Aptekar et al. *GCN*, **20292** (2016).
12. D.S. Svinkin, D.D. Frederiks, R.L. Aptekar et al., *ApJS*, **224**, 10 (2016).
13. D.E. Reichart, D.Q. Lamb, E.E. Fenimore et al., *ApJ*, **552**, 57 (2001).
14. C. Guidorzi, F. Frontera, E. Montanari et al., *MNRAS*, **363**, 315 (2005).
15. S. Dichiara, C. Guidorzi, L. Amati et al., *MNRAS*, **431**, 3608 (2013).
16. C. Guidorzi, S. Dichiara and L. Amati, *A&A*, **589**, A98 (2016).
17. J.P. Norris, G.F. Marani and J.T. Bonnell, *ApJ*, **534**, 248 (2000).
18. T.N Ukwatta, M. Stamatikos, K.S. Dugha et al., *ApJ*, **711**, 1073 (2011).
19. R. Margutti, C. Guidorzi, G. Chincarini et al., *MNRAS*, **406**, 2149 (2010).
20. M.G. Bernardini, G. Ghirlanda, S. Campana et al., *MNRAS*, **446**, 1129 (2015).
21. D. Kocevski and E. Liang, *ApJ*, **594**, 385 (2003).
22. LIGO Scientific Collaboration and Virgo Collaboration, *ApJ*, **848**, L13 (2017).